



Highly enantioselective olefin epoxidation controlled by helical confined environments



Cristina I. Fernandes^a, Marta S. Saraiva^a, Teresa G. Nunes^b, Pedro D. Vaz^{a,*}, Carla D. Nunes^{a,*}

^a CQB, Departamento de Química e Bioquímica, Faculdade de Ciências da, Universidade de Lisboa, 1749-016 Lisboa, Portugal

^b Centro de Química Estrutural, Universidade de Lisboa, Instituto Superior Técnico, Av. Rovisco Pais, 1049-001 Lisboa, Portugal

ARTICLE INFO

Article history:

Received 18 July 2013

Revised 23 August 2013

Accepted 27 August 2013

Keywords:

Asymmetric catalysis
Chiral recognition
Helical materials
Molybdenum
Olefin epoxidation
Stereoselectivity
Mesoporous materials
Oxidation catalysis

ABSTRACT

Helical mesoporous materials of the MCM-41 type are important materials that can be prepared by one-pot synthesis procedures with a co-surfactant. A control of the characteristics at a local level is of the most important in the view of the applications of such materials. However, there are not many studies relating such features with synthetic approaches. In this work, we prepared both helical and regular channel materials from Si-based MCM-41 type. Afterward, a bpy derivative was used as ligand to coordinate Mo^{IV/VI}. The complexes and the new materials were tested as the catalytic precursors in the epoxidation of *cis*-cyclooctene, styrene, 1-octene, *R*-(+)-limonene and *trans*-hex-2-en-1-ol, using tert-butylhydroperoxide (TBHP) as oxidant. Although almost all the catalysts were 100% selective toward the epoxide, the conversions were in general good. The major achievement of these catalysts is an outstanding stereocontrol of the reaction products. In addition, these catalysts were found to be very effective under several circumstances. This is certainly an important contribution for such concept and may render such materials further applications where chiral recognition is important.

© 2013 Elsevier Inc. All rights reserved.

1. Introduction

Olefin epoxidation is very important in the preparation of relevant building blocks for organic synthesis or polymer science [1–3]. Among several processes developed for asymmetric oxidation of olefins, one of the earliest was that by Sharpless using a Ti^{IV} catalyst in the presence of tartrate, especially effective with allylic alcohols [4,5]. The Jacobsen–Katsuki epoxidation was later reported relying on the use of a Mn–salen catalyst [6,7]. Both methods were important milestones in olefin epoxidation although they present some drawbacks such as being less reactive and selective toward *Z*-olefins (Sharpless) or require low (ca. 273 K) reaction temperatures (Jacobsen–Katsuki) [8]. Shibasaki reported asymmetric epoxidation reactions based on a La(BINOL) catalyst [9]. This reaction shows an improvement over the previous ones as it can proceed under mild conditions (r.t.), and it also works reasonably well with *Z*-olefins [10,11]. A number of metal-free alkene oxidation methods have also been reported. The Shi epoxidation reaction relies on the use of a fructose-based chiral dioxirane to conduct the transformation [12,13]. While it shows to be active on a wide scope of substrates, as a shortcoming, it requires high catalyst loadings to achieve good yields. The Juliá–Colonna is also

a widely employed method based on the use of poly-amino acids, which was reported some time ago [14,15]. Although it was developed over a relatively narrow range of substrates initially, it has suffered major improvements in recent times [10,11].

Almost all effective ligands reported for homogeneous catalytic reactions share one prominent common feature – a rigid and bulky structure that is vital to create effective asymmetric microenvironments around the catalytically active site. By the same token of confinement effects, solid surfaces have been used with success to promote heterogeneous asymmetric catalysis, thus preserving or improving the high enantioselectivity of product *ee* values compared to their homogeneous analogues [16–23]. More recently, chiral helical polymers, reported by Suginome and coworkers, were used in asymmetric reactions with stereocontrol induced by the helical backbone [24–27].

To this respect, the preparation of nanostructured materials with helical morphology opened a new field of research due to their potential applications such as chiral selective separation and recognition and enantioselective catalysis [28–32]. Still, a drawback is the lack of active sites of mesoporous materials, which does not exclude the helical silica-based materials as well. To circumvent this, flav different strategies are available to introduce such active sites, ranging from co-condensation or post-synthesis procedures to matrix doping for introduction of such active species [33,34].

* Corresponding authors. Fax: +351 217 500088.

E-mail addresses: pmvaz@fc.ul.pt (P.D. Vaz), cmnunes@fc.ul.pt (C.D. Nunes).

As part of our ongoing research toward more efficient and selective systems based on single-site active species which allow a fast inflow of reactants and outflow of products [35], we report for the first time – to the best of our knowledge – the incorporation of $\text{Mo}^{\text{II/VI}}$ active species inside pores of left-handed helical mesostructured silica materials [32]. The Mo-derivatized helical materials led to highly active heterogeneous catalysts for asymmetric oxidation of olefins and were benchmarked with similar Mo homogeneous complexes.

Molybdenum catalysts are known for being very effective catalysts in olefin epoxidation reactions [36–43]. Although many efforts have been addressed concerning development of asymmetric reactions, only a few were successful [39–43]. Some authors have inclusively mentioned some reasons for this [40,42].

In addition, the helical host materials reported here have Lewis and Brønsted acid properties due to the template extraction procedure (based on an extraction using methanol acidified with HCl instead of calcination) as reported by us recently for related materials [35,44].

For benchmarking purposes and to understand the role of the helical matrix in the catalytic performance, regular MCM-41 materials were also prepared.

2. Experimental

2.1. Catalysts preparation

All reagents were obtained from Aldrich and used as received. Commercial grade solvents were dried and deoxygenated by standard procedures distilled under nitrogen and kept over 4 Å molecular sieves (3 Å for acetonitrile). The complexes $[\text{Mo}_2(\text{CO})_3(\text{CH}_3\text{CN})_2]$, $[\text{MoO}_2\text{Cl}_2(\text{thf})_2]$ and $\text{Me}_2\text{bpy-Mo}^{\text{VI}}$ were prepared according to the literature methods [45–47]. The $(\text{ClCO})_2\text{bpy}$ ligand (4,4'-dicarbonyl-2,2'-bipyridine chloride) was obtained from the corresponding carboxylic acid (4,4'-dicarboxylic-2,2'-bipyridine), which had previously been obtained by oxidation of the methyl derivative (4,4'-dimethyl-2,2'-bipyridine) [48].

The complex $\text{Me}_2\text{bpy-Mo}^{\text{II}}$ was prepared by adding a methanol solution (10 mL) of 4,4'-dimethyl-2,2'-bipyridine (Me_2bpy) (0.092 g; 0.5 mmol) to a methanol solution (10 mL) of the precursor complex $[\text{Mo}_2(\text{CO})_3(\text{CH}_3\text{CN})_2]$ (0.258 g; 0.5 mmol). The resulting solution was stirred for 14 h at r.t. under inert atmosphere. After, the solution was filtered off and the solid washed with dichloromethane (CH_2Cl_2) and dried under vacuum for 4 h at 323 K.

The helical mesostructured silica materials (MS_h), two batches, were prepared using an entropy-driven procedure with achiral cationic surfactant templates. In this case, we used cetyltrimethylammonium bromide (C_{16}TAB) and ammonia as surfactant and co-surfactant, respectively, according to a literature procedure [32]. In a typical catalyst synthesis procedure, 0.4 g of C_{16}TAB (Fluka, 96.0%) was dissolved in 50 mL of aqueous ammonia solution (Sigma-Aldrich, 25 wt%) at 313 K. Then, 2.0 mL of tetraethoxysilane (TEOS) (Aldrich, 98%) was added to the solution. The sol was allowed to react for 3 h at that temperature under stirring (800 rpm). After this period, the mixture was transferred to a Teflon-lined stainless steel autoclave and aged at 373 K for 24 h.

Two batches of MCM-41 (hereafter denoted as MS) were synthesized as well, one for each Mo species. Both MCM-41 were synthesized by adopting a methodology previously described, using $[(\text{C}_{14}\text{H}_{33})\text{N}(\text{CH}_3)_3]\text{Br}$ as structure directing agent [35].

To remove the surfactant, the MS_h and MS materials (3 g) were added to a solution of MeOH (250 mL) and HCl 36% (6.0 g). After stirring for 6 h at 323 K, the solid was filtered off and dried in vacuum during 2 h.

Prior to the grafting experiments, physisorbed water was removed from the materials by heating at 453 K in vacuum (10^{-2} Pa) for 2 h.

Materials $\text{MS}_h\text{-bpy}$ and MS-bpy resulted from the addition of a suspension of the $(\text{ClCO})_2\text{bpy}$ ligand (0.281 g; 1 mmol) in acetonitrile (CH_3CN) to either a MS_h or MS suspension (1 g) in acetonitrile (CH_3CN), and the mixture was heated at 358 K for 14 h. The resulting solid was filtered off and washed twice with dichloromethane (CH_2Cl_2) and then dried in vacuum at 323 K for 2 h. $\text{MS}_h\text{-bpy-Mo}^{\text{II}}$ and $\text{MS}_h\text{-bpy-Mo}^{\text{VI}}$ materials were obtained by adding a solution of $[\text{Mo}_2(\text{CH}_3\text{CN})_2(\text{CO})_3]$ (0.300 g, 0.56 mmol) or $[\text{MoO}_2\text{Cl}_2(\text{thf})_2]$ (0.300 g, 0.87 mmol) in dry dichloromethane (CH_2Cl_2) to a suspension of 1 g of $\text{MS}_h\text{-bpy}$ material in dry dichloromethane (CH_2Cl_2). The reaction mixture was stirred under a N_2 atmosphere at room temperature for 14 h. The resulting material was then filtered off, washed twice with dichloromethane (CH_2Cl_2), and dried under vacuum for 3 h. The corresponding $\text{MS-bpy-Mo}^{\text{II}}$ and $\text{MS-bpy-Mo}^{\text{VI}}$ materials were also obtained by similar procedure.

2.2. Catalysts characterization

FTIR spectra were obtained either as KBr pellets (complexes) or Diffuse Reflectance (DRIFT) measurements (materials) on a Nicolet 6700 in the 400–4000 cm^{-1} range using 2 cm^{-1} resolution. Powder XRD measurements were taken on a Philips Analytical PW 3050/60 X'Pert PRO (theta/2 theta) equipped with X'Celerator detector and with automatic data acquisition (X'Pert Data Collector (v2.0b) software), using a monochromatized $\text{Cu K}\alpha$ radiation as incident beam, using 40 kV and 30 mA. ^1H and ^{13}C solution NMR spectra were obtained with a Bruker Avance 400 spectrometer at room temperature.

Solid-state NMR measurements were performed at room temperature on a Bruker MSL 300P spectrometer operating at 59.60 and 75.47 MHz for the observation of ^{29}Si and ^{13}C resonances, respectively. The standard magic angle spinning (MAS) cross-polarization–dipolar decoupling RF pulse sequence (CP–DD) was carried out at ca. 4 kHz spinning rate. For the acquisition of ^{29}Si spectra, 5 ms contact time, 6 s recycling delay, and a number of scans always higher than 3000 were selected; the Hartmann–Hahn condition was optimized using tetrakis(trimethylsilyl)silane, and tetramethylsilane (tms) was the external reference to set the chemical shift scale ($\delta = 0$). ^{13}C spectra were recorded with 2 ms contact time, 4 s recycling delay, and a number of scans higher than 900. The Hartmann–Hahn condition was optimized using glycine, also the external reference to set the chemical shift scale (^{13}CO at 176.1 ppm).

The N_2 sorption measurements were obtained in an automatic apparatus (ASAP 2010; Micromeritics). BET specific surface areas (S_{BET} , p/p_0 from 0.03 to 0.30) and specific total pore volume V_p were estimated from N_2 adsorption isotherms measured at 77 K. The pore size distributions (PSD) were calculated by the BJH method using the modified Kelvin equation with correction for the statistical film thickness on the pore walls [49,50]. The statistical film thickness was calculated using Harkins–Jura equation in the p/p_0 range from 0.1 to 0.95.

Microanalyses for CHN and Mo quantification were performed at CACTI, University of Vigo. CHN analyses were performed on a Fisons EA 1108; Mo quantification was performed on a Perkin Elmer Optima 4300DV using In as internal standard.

SEM images were obtained on a FEG-SEM (Field Emission Gun Scanning Electron Microscope) from JEOL, model JSM-7001F. TEM images were obtained on a Hitachi microscope, model H-8100 with a LaB_6 filament using an acceleration tension of 200 kV.

2.3. Catalytic tests

The complexes and materials were tested in the epoxidation of olefins and allylic alcohols, such as *cis*-cyclooctene, styrene, 1-octene, *trans*-hex-2-en-1-ol, and *R*-(+)-limonene, using *t*-butylhydroperoxide (tbhp) as oxidant (Aldrich, 5.5 M in *n*-decane). The catalytic oxidation tests were carried out at 328 K under air in a reaction vessel equipped with a magnetic stirrer and a condenser. In a typical experiment, the vessel was loaded with olefin or alcohol (100 mol%), internal standard (dibutyl ether, dbE), catalyst (1 mol%), oxidant (200 mol%), and 3 mL of dichloromethane as solvent. The final volume of the reaction is ca. 6 mL. Addition of the oxidant determines the initial time of the reaction. Conversion, product yields and stereochemistry were monitored by sampling periodically and analyzing them using a Shimadzu QP2100-Plus GC/MS system and a capillary column (Teknokroma TRB-5MS/TRB-1MS or Restek Rt- β DEXsm) operating in the linear velocity mode. All reactions were conducted under normal atmosphere. *R*-(+)-limonene epoxidation was carried out at different temperatures, 328 K, 353 K, and 393 K, using dichloromethane, ethanol, and toluene as solvents, respectively.

2.4. Leaching and recycling tests

In general, these experiments were carried out as described in the previous section for cyclooctene and *R*-(+)-limonene epoxidation using material MS_h -*bpy*- Mo^{II} as catalyst; conversion and product yields were monitored as described above in Section 2.3.

For the leaching experiments after 2 h reaction, the catalyst was filtered off, and the reactions continued under the same conditions. In the case of the recycling experiments, after each cycle (24 h), the catalyst was filtered, washed with CH_2Cl_2 , and dried prior to reuse in a new catalytic cycle.

2.5. Study on chirality of MS_h materials

This study was based on a literature protocol with slight alterations (phenylalanine was used instead of valine) [51]. A solution of 50 mg of pure *L*-phenylalanine (or *D*-phenylalanine) was dissolved in 20 mL of MilliQ water followed by adding 20 mg of template-free MS_h material previously activated. The mixture was magnetically stirred under ambient conditions and at a constant temperature of 298 K. The concentration of *L*-phenylalanine (or *D*-phenylalanine) was measured using UV spectroscopy (absorption at 260 nm) by sampling at regular time intervals. The procedure was applied to 5 different batches of MS_h materials, and each one was tested in triplicate.

3. Results and discussion

3.1. Synthesis and characterization of homogeneous catalysts

4,4'-Dicarbonyl-2,2'-bipyridine chloride was obtained by reaction of 4,4'-dimethyl-2,2'-bipyridine (Me_2bpy) with concentrated sulfuric acid (H_2SO_4) and chromium oxide (CrO_3) [48]. The $(CO_2H)_2bpy$ intermediary product was characterized by 1H and ^{13}C NMR in its sodium salt form using deuterated water as solvent and was found to be similar to the literature report [48].

After that, reaction of the obtained product $(CO_2H)_2bpy$ with thionyl chloride ($SOCl_2$) yields the desired product adopting a literature procedure [52]. The compound was used without isolation for the derivatization of the MS_h materials, since it decomposes promptly when exposed to air (see Scheme 1).

The complexes $Me_2bpy-Mo^{II}$ and $Me_2bpy-Mo^{VI}$ were prepared from $[MoI_2(CO)_3(CH_3CN)_2]$ or $[MoO_2Cl_2(thf)_2]$ with 4,4'-dimethyl-

2,2'-bipyridine (Me_2bpy) in 1:1 ratio, in methanol or dichloromethane (Scheme 2).

They were characterized by elemental analysis, FTIR, and 1H NMR spectroscopy. Elemental analysis of the $Me_2bpy-Mo^{II}$ and $Me_2bpy-Mo^{VI}$ complexes is shown in Table 1. As can be seen, both complexes were synthesized successfully as formulated with experimental values matching closely expected values. For the $Me_2bpy-Mo^{VI}$ complex, our experimental values are also in agreement with the literature data [47].

The 1H NMR spectra of $Me_2bpy-Mo^{II}$ and $Me_2bpy-Mo^{VI}$ complexes are presented in Table 2. The changes experienced by the protons are in some cases very clear as shown in Table 2 which summarizes the observed chemical shift for complexes $Me_2bpy-Mo^{II}$ and $Me_2bpy-Mo^{VI}$ and comparison with the free ligand. As can be seen from Table 2, all signals shift downfield in the complexes compared to the free Me_2bpy ligand. This is most probably due to the presence of the Mo centers that cause a lower electron density at the ligand. The ^{13}C NMR spectra were not recorded due to low solubility.

Characterization by vibrational spectroscopy was also accomplished to track formation of the complexes, according to Fig. 1. In $Me_2bpy-Mo^{II}$ complex, the strong absorptions of the $\nu_{C=O}$ modes are clearly observed at 2026, 1963, and 1916 cm^{-1} , confirming the presence of the $[MoI_2(CO)_3]$ core.

In complex $Me_2bpy-Mo^{VI}$, some characteristic bands are also observed. The symmetric and asymmetric Mo=O stretching modes are observed as a couple of strong bands at 944 and 917 cm^{-1} , respectively. These bands confirm the presence of the $[MoO_2Cl_2]$ core and that the initial Mo^{VI} oxidation state is preserved. Another important probe for Mo coordination is the $\nu_{C=N}$ mode of Me_2bpy . In fact, in the free form, it appears at 1691 cm^{-1} while after coordination to Mo, it redshifts to 1617 and 1614 cm^{-1} in $Me_2bpy-Mo^{II}$ and $Me_2bpy-Mo^{VI}$, respectively.

Characterization of complex $Me_2bpy-Mo^{II}$ by elemental analysis confirmed its formulation as proposed in Scheme 2.

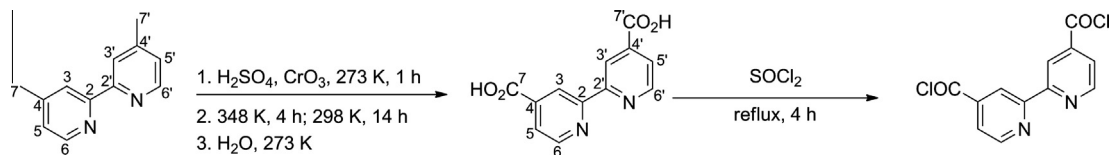
3.2. Synthesis and characterization of heterogeneous catalysts

The regular MCM-41 type mesostructured silica materials (MS) were prepared using myristyltrimethylammonium bromide ($C_{14}TAB$) as surfactant, according to a literature procedure [35]. All subsequent derivatization operations were similar to those made for the MS_h helical materials. Therefore, we will only describe the procedure for the latter.

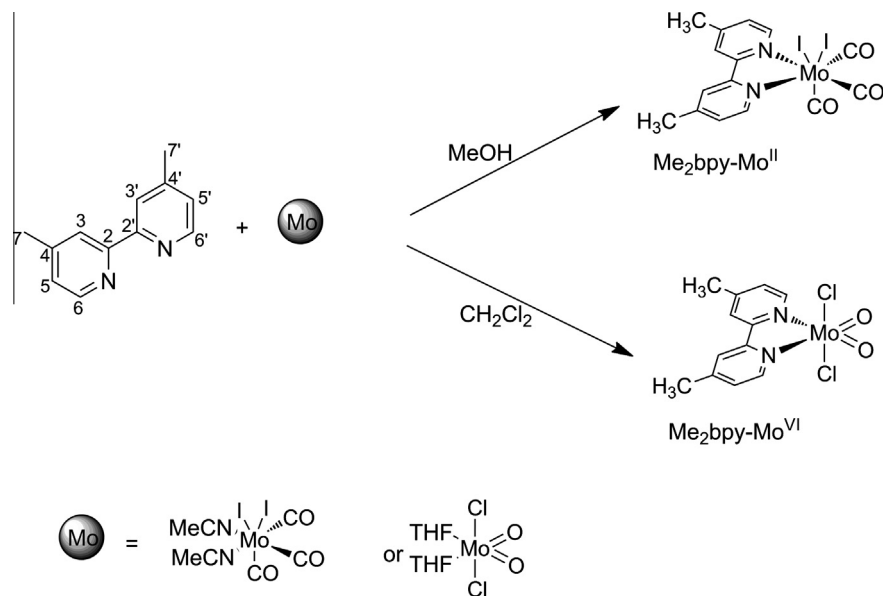
The helical mesostructured silica materials (MS_h) were prepared using an entropy-driven procedure with achiral cationic surfactant template and ammonia. In this particular case, we used cetyltrimethylammonium bromide ($C_{16}TAB$) and ammonia as surfactant and co-surfactant, respectively, according to a literature procedure [32].

Afterward, a bipyridine (*bpy*) derivative (Scheme 3) was used as ligand to coordinate $Mo^{II/VI}$ centers after being grafted to the inner silanol surface of the material. Two batches were produced: one for preparing the Mo^{II} catalyst and another for the Mo^{VI} counterpart.

Grafting of *bpy* ligand was straightforward by reacting $(ClCO)_2bpy$ with a suspension of MS_h in acetonitrile. Afterward, the Mo^{II} and Mo^{VI} centers were introduced by suspending the MS_h -*bpy* materials in dichloromethane and then adding the precursor complexes, either $[MoI_2(CO)_3(CH_3CN)_2]$ or $[MoO_2Cl_2(thf)_2]$. This afforded both MS_h -*bpy*- Mo^{II} and MS_h -*bpy*- Mo^{VI} materials, and according to elemental analysis, the Mo contents were found to be 4.26% and 1.21%, corresponding to 0.45 mmol g^{-1} and 0.13 mmol g^{-1} , respectively. CHN analyses for MS_h -*bpy*- Mo^{II} and MS_h -*bpy*- Mo^{VI} revealed values of 11.93 %C, 1.78 %H, and 1.76 %N for the former and 6.46 %C, 2.0 %H, and 1.10 %N for the latter. Based on the N content, these results also show that the loading of *bpy*



Scheme 1. Synthesis of ligand $(ClCO)_2bpy$ for further functionalization of MS_h materials. Numbering scheme refers to NMR assignment.



Scheme 2. Synthesis of complexes $Me_2bpy-Mo^{II}$ and $Me_2bpy-Mo^{IV}$.

Table 1
CHN elemental analysis of Mo complexes.

Complex	Calculated			Experimental		
	C	H	N	C	H	N
$Me_2bpy-Mo^{II}$	29.15	1.96	4.53	28.99	2.11	4.60
$Me_2bpy-Mo^{IV}$	37.62	3.16	7.31	37.45	3.62	7.44

Table 2
 1H chemical shifts for Me_2bpy ligand and respective complexes $Me_2bpy-Mo^{II}$ and $Me_2bpy-Mo^{IV}$.

δ (ppm)	H ₃	H ₅	H ₆	H ₇
Me_2bpy	8.23	7.11	8.52	2.42
$Me_2bpy-Mo^{II}$	9.16	8.10	9.18	2.63
$Me_2bpy-Mo^{IV}$	8.51	7.67	8.71	3.47

derivative inside the pores is 1.15 mmol g^{-1} and 0.72 mmol g^{-1} , respectively. By the same token for $MS-bpy-Mo^{II}$ and $MS-bpy-Mo^{IV}$ materials, CHN analyses revealed values of 7.34 %C, 1.37 %H, and 0.98 %N for the former and 12.31 %C, 1.75 %H, and 1.42 %N for the latter. Based on the N content, these results also show that the loading of *bpy* derivative inside the pores is 0.64 mmol g^{-1} and 0.93 mmol g^{-1} , respectively. The Mo content for these materials was found to be 4.36% and 4.97%, corresponding to 0.45 mmol g^{-1} and 0.52 mmol g^{-1} , by the same order.

All materials were conveniently characterized by DRIFT, powder XRD, SEM and TEM, and ^{29}Si and ^{13}C CP-MAS SS/NMR. Sorption/desorption N_2 isotherms were also carried out for textural parameters estimation. All spectroscopic/textural characterization features discussed in the following lines were found to be in agreement with related hybrid matrix mesoporous materials. The

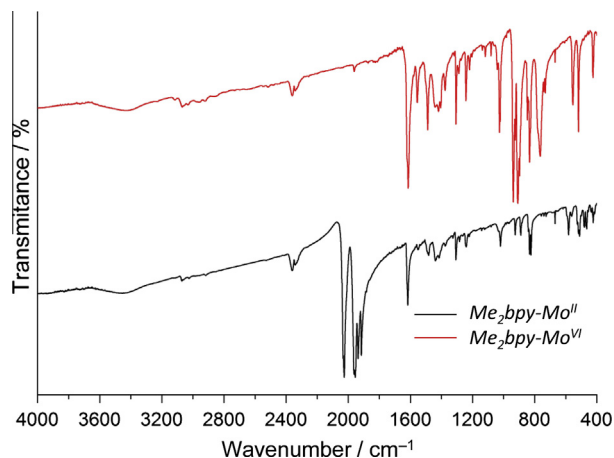


Fig. 1. FTIR spectra of $Me_2bpy-Mo^{II}$ and $Me_2bpy-Mo^{IV}$ complexes.

helical matrices of the as-prepared MS_h materials were confirmed by SEM and TEM measurements Fig. 2. The SEM image shows that MS_h materials consist of rod-like particles. The length of the rods ranges from hundreds of nanometers to $2 \mu\text{m}$, whereas the rod diameter varies from 80 to 150 nm. TEM images confirm the helical morphology and illustrate the periodic appearance of lattice fringes (Fig. 2, right) along the rods, indicating the presence of helical channels within the rods [31,32]. The periodicity of the lattice fringes indicates that there is a regular environment of the channels where reactants and products may diffuse along without much disturbing.

The local structure was also confirmed by powder X-ray diffraction measurements, which agree with the published data and also

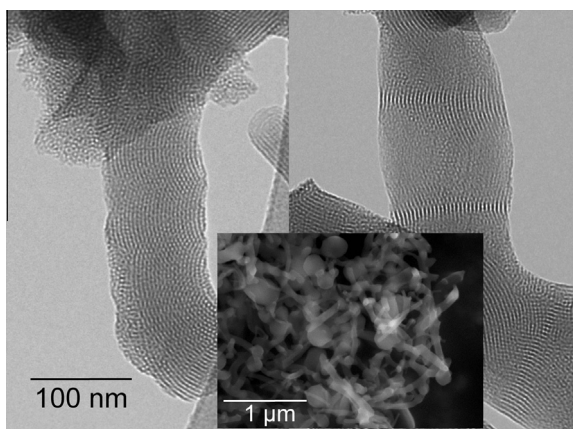
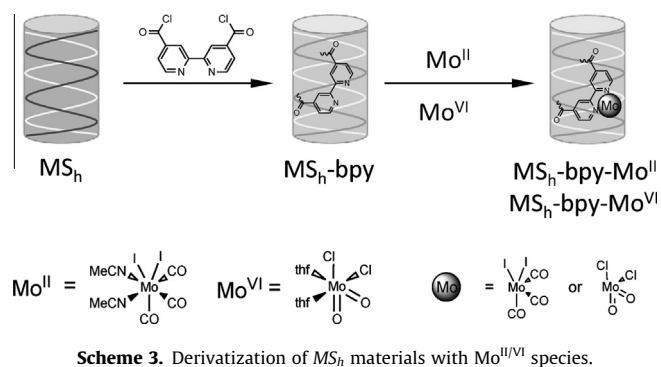


Fig. 2. TEM images of MS_h materials. The inset shows a SEM image of the particles.

make possible to verify that materials MS_h -bpy and MS_h -bpy- $Mo^{II/VI}$ are mesostructured.

All resulting materials were of good quality according to the X-ray diffraction (XRD) powder patterns (Fig. 3).

The XRD powder patterns of the chiral MS_h , pristine materials exhibit four reflections indexed to a hexagonal cell as (100), (110), (200), and (210) in the 2 – 10° 2θ range. For material MS_h , the d_{100} value for reflection (100) is estimated to be 42.3 Å, corresponding to a lattice constant of $a = 48.8$ Å ($a = 2d_{100}/\sqrt{3}$). Materials MS_h -bpy and MS_h -bpy- Mo^{II} , obtained after subsequent stepwise functionalization with bpy and Mo^{II} , still show three reflections although with a slight deviation of the position maxima toward higher 2θ values as compared to MS_h . For MS_h -bpy material, the

d_{100} value is 42.4 Å with a corresponding lattice constant of $a = 49.0$ Å; for MS_h -bpy- Mo^{II} , the values are, respectively, $d_{100} = 41.2$ Å and $a = 48.4$ Å. Similar observations were made for the set of materials MS_h , MS_h -bpy, and MS_h -bpy- Mo^{VI} used for the Mo^{VI} derivatives. In the case of the MS materials, XRD powder patterns were found to provide similar results to those already reported by us for related systems [35,44,52]. Despite this, all data from all materials are collected in Table 3, summarizing the relevant textural properties of all materials leading to the preparation of both Mo^{II} and Mo^{VI} derivatives. The observed peak intensity reduction is common to all materials; it is even more significant in the materials with the Mo cores. This is not due to a crystallinity loss, but rather to an X-ray scattering contrast reduction between the silica walls and the pore-filling material. This has been observed for other types of materials and is well described in the literature [53,54].

Nitrogen sorption/desorption studies at 77 K were performed and have revealed that MS_h samples exhibit a reversible type IV isotherm (Fig. 4), typical of mesoporous solids (pore width between 2 nm and 50 nm, according to IUPAC) [55]. The calculated textural parameters (S_{BET} and V_p) of these materials (Table 3) agree with the literature data [56,57]. The capillary condensation/evaporation step in pristine MS_h samples appears in the 0.34–0.44 relative pressures range, while the sharpness of this step reflects a uniform pore size distribution.

The functionalized material MS_h -bpy isotherm revealed much lower N_2 uptake, accounting for the decreases in both S_{BET} (18% and 14%) and V_p (14% and 19%), according to Table 3. These findings indicate that the ligand immobilization on the internal silica surface was accomplished (Fig. 4, Table 3). For the MS_h -bpy- Mo^{II} material, the S_{BET} and V_p relative decrease related to MS_h is 31% and 29%, respectively. This result is in agreement with the p/p^0 coordinate decrease in the isotherm inflection points after post-synthesis treatments [58]. Furthermore, the maximum of the PSD curve (Fig. 4) determined by the BJH method, d_{BJH} , for MS_h material changes from 35.3 Å to 34.4 Å (Table 3). For the MS_h -bpy- Mo^{VI} material, the relative decrease in S_{BET} and V_p when compared to MS_h is 27% for both parameters. These are in line with those described above for the other set of materials.

Textural parameters for MS materials (Table 3) were also found to match values reported in the literature for related systems [35,44,52] and comparable to those described above for MS_h materials.

Diffuse reflectance infrared spectroscopy (DRIFT) was used to characterize the hybrid materials, shown in Fig. 5.

The DRIFT spectrum of the MS_h host material is typical of a silicate evidencing a broad band in the 3600 – 2600 cm^{-1} range due to

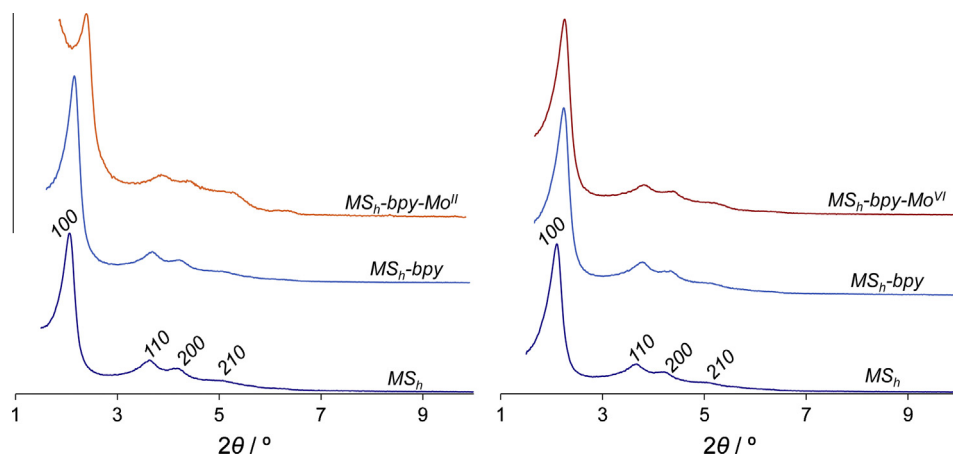


Fig. 3. Powder XRD of MS_h , MS_h -bpy, MS_h -bpy- Mo^{II} and MS_h -bpy- Mo^{VI} materials.

Table 3
Textural parameters of host and composite materials, from powder XRD data and N₂ isotherms at 77 K, for all prepared mesoporous materials.

Material	2θ (°)	d ₁₀₀ (Å)	a (Å)	S _{BET} (m ² g ⁻¹)	ΔS _{BET} ^a (%)	V _p (cm ³ g ⁻¹)	ΔV _p ^b (%)	d _{BH} (Å)
MS	2.26	39.0	45.0	897	–	0.75	–	34.3
MS- <i>bpy</i>	2.47	35.5	41.0	818	–9	0.62	–17	31.9
MS- <i>bpy</i> -Mo ^{II}	2.49	36.1	41.6	755	–16	0.59	–21	32.8
MS	2.22	39.7	45.8	982	–	0.85	–	34.3
MS- <i>bpy</i>	2.26	39.1	45.2	914	–7	0.79	–7	32.6
MS- <i>bpy</i> -Mo ^{VI}	2.30	38.5	44.4	682	–31	0.75	–12	31.1
MS _h	2.08	42.3	48.8	949	–	0.83	–	35.3
MS _h - <i>bpy</i>	2.08	42.4	49.0	775	–18	0.71	–14	34.5
MS _h - <i>bpy</i> -Mo ^{II}	2.11	41.2	48.4	657	–31	0.59	–29	34.4
MS _h	2.12	41.6	48.0	994	–	0.85	–	36.1
MS _h - <i>bpy</i>	2.12	41.5	47.9	859	–14	0.69	–19	35.4
MS _h - <i>bpy</i> -Mo ^{VI}	2.13	41.7	48.2	728	–27	0.62	–27	35.3

^a Surface area variation relatively to parent MS_h.

^b Total pore volume variation relatively to parent MS_h.

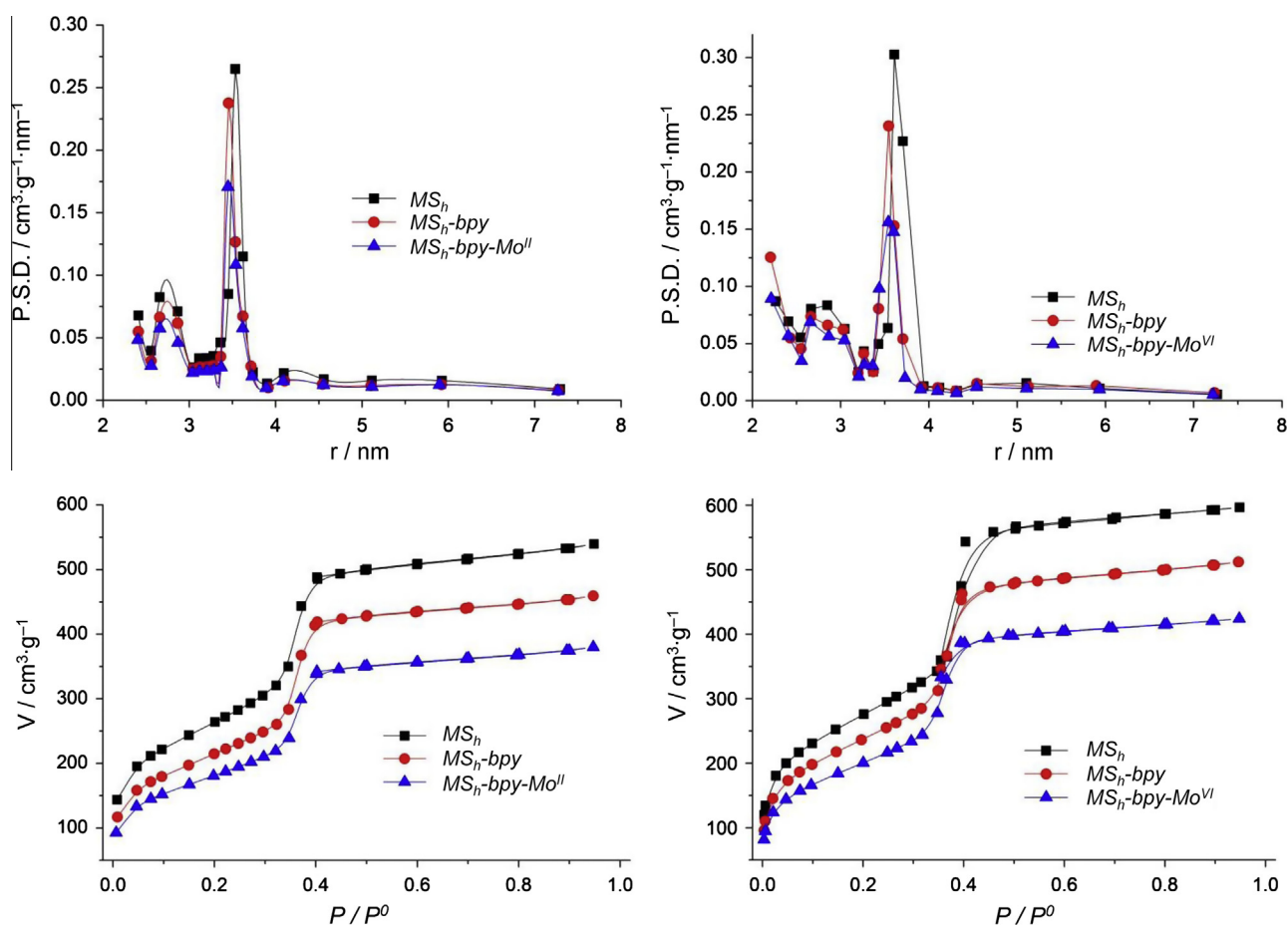


Fig. 4. Nitrogen adsorption studies of MS_h, MS_h-*bpy*, MS_h-*bpy*-Mo^{II} and MS_h-*bpy*-Mo^{VI} materials at 77 K: isotherms (bottom) and pore size distribution curves (top).

hydrogen bonding silanol groups. A sharp band at 3674 cm⁻¹ is due to silanol groups not involved in hydrogen bonding. Other important features comprise the band at ca. 1634 cm⁻¹ due to OH bending modes, while the intense broad band at 1239–950 cm⁻¹ is assigned to the asymmetric stretching vibration modes of the mesoporous framework (νSi–O–Si) [59]. After grafting of ligand *bpy*, which affords the material MS_h-*bpy*, the DRIFT spectrum shows an overall similar profile dominated by the absorptions of the host mesoporous material. Additionally, new bands were detected evidencing the ligand presence within the pores. The

1634 cm⁻¹ band can be related with the νC=N mode in addition to the OH bending mode of the matrix. Grafting of the *bpy* ligand was also monitored by probing its νC=O mode. The (ClCO)₂*bpy* ligand shows this mode at 1730 cm⁻¹, which agrees with the presence of the COCl group. After grafting, this mode is redshifted to 1713 cm⁻¹, which is compatible with the expected transformation resulting in the formation of silyl esters, as documented in the literature [60]. In this way, the absence of the 1730 cm⁻¹ band in the MS_h-*bpy* and MS-*bpy* materials strongly suggest that the *bpy* ligand is grafted to the inorganic matrix in a bipodal fashion.

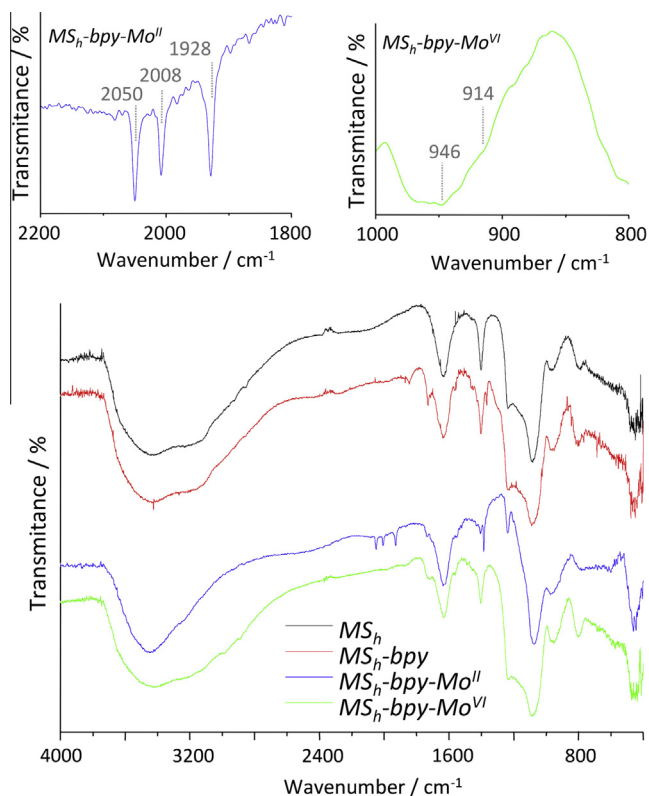


Fig. 5. Infrared spectra of MS_h , MS_h -bpy, MS_h -bpy- Mo^{II} and MS_h -bpy- Mo^{VI} materials. The top images show a zoomed image of the $\nu C\equiv O$ and $\nu Mo=O$ modes region from MS_h -bpy- Mo^{II} and MS_h -bpy- Mo^{VI} materials, respectively.

After binding the molybdenum complexes $[Mo_2(CO)_3(CH_3CN)_2]$ and $[MoO_2Cl_2(thf)_2]$, which afford materials MS_h -bpy- Mo^{II} and MS_h -bpy- Mo^{VI} , respectively, several changes/additional bands in the corresponding DRIFT spectra are detected. In what concerns material MS_h -bpy- Mo^{II} , the most remarkable feature is the observation of three bands at 2050, 2008, and 1928 cm^{-1} assigned to the $\nu C\equiv O$ modes. These bands are inclusively shifted relatively to the $[Mo_2(CO)_3(CH_3CN)_2]$ precursor complex. This is indicative of the metal-ligand binding. Additionally, the bands due to the $\nu C\equiv N$ vibrational modes from the acetonitrile (CH_3CN) ligands are not found, indicating that such ligands have been replaced by the immobilized ligand.

The most relevant spectral feature for the MS_h -bpy- Mo^{VI} material is a pair of bands observed at 946 and 914 cm^{-1} assigned to the $\nu Mo=O$ modes of the $[MoO_2Cl_2]$ core.

The FTIR spectra of the MS -bpy- Mo^{II} and MS -bpy- Mo^{VI} materials show the presence of above-mentioned bands. In this way, the $\nu C\equiv O$ modes in MS -bpy- Mo^{II} are observed at 2040, 1997 and 1930 cm^{-1} . In the case of MS -bpy- Mo^{VI} material, the $\nu Mo=O$ modes are observed at 946 and 914 cm^{-1} .

Fig. 6 shows the ^{29}Si CP-MAS NMR spectra for pristine MS_h and the derivatized MS_h -bpy, MS_h -bpy- Mo^{II} , and MS_h -bpy- Mo^{VI} materials.

Unmodified MS_h displays two broad convoluted resonances in the ^{29}Si CP-MAS NMR spectrum at -101 and -110 ppm, assigned to Q^4 and Q^3 species of the silica framework, respectively [$Q^n = -Si(OSi)_n(OH)_{4-n}$]. A weak shoulder is also observed at -91 ppm due to the Q^2 species. The Q^3 sites are associated with single silanols $Si-OH$ (including hydrogen-bonded silanols), whereas the Q^2 sites correspond to geminal silanols [$Si(OH)_2$]. The ^{29}Si CP-MAS spectrum of MS_h -bpy also displays three broad signals at -94 , -101 , and -109 ppm, assigned to Q^2 , Q^3 and Q^4 organosilicon species, respectively.

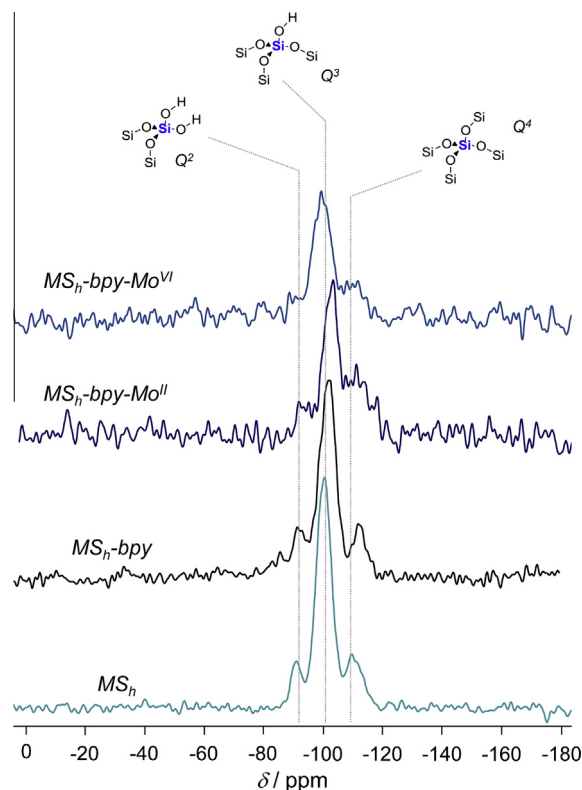


Fig. 6. ^{29}Si CP-MAS NMR spectra for MS_h , MS_h -bpy, MS_h -bpy- Mo^{II} and MS_h -bpy- Mo^{VI} materials.

According to Fig. 6, reaction of MS_h with $(ClCO)_2bpy$ ligand and the (organo)metallic fragments $[Mo_2(CO)_3]$ and $[MoO_2Cl_2]$ did not significantly change the ^{29}Si CP-MAS spectrum, as expected, indicating that the metal fragment reacted with the immobilized ligand and did not interact with the wall surface. Comparing the three materials prepared by this approach, the in situ grafting of ligand bpy in MS_h affording MS_h -bpy results in the reduction of the Q^2 and Q^3 resonances. Similar results were obtained for the corresponding MS materials, which show as well the same changes described for the MS_h ones.

The ^{13}C CP-MAS SS-NMR spectra (not shown) of the MS_h -bpy and MS_h -bpy- Mo^{II} materials are quite similar to those of the bpy ligand, confirming its binding to the surface. The same was observed for the corresponding series of MS materials.

3.3. Catalytic studies

The catalytic activity of the MS_h and MS materials and related homogeneous counterparts was benchmarked in olefin epoxidation using *t*-butylhydroperoxide (tbhp) as oxygen source. The comparison with homogeneous catalysts should be made with some caution as the Me_2bpy ligand has electron donor properties while the $CObpy$ in the materials shows electron withdrawing ones. Despite this, the homogeneous catalysts perform quite well in conversion terms.

Special focus was dedicated to stereoselectivity of products due to the specific helical features of the matrix. In this way, we have tested the catalysts in the epoxidation of cyclooctene, styrene, 1-octene, *trans*-hex-2-en-1-ol, and *R*-(+)-limonene (Table 4). Blank runs (without catalyst and in the presence of oxidizing agent) gave virtually no conversion of starting material.

In the case of cyclooctene, both MS_h -bpy- $Mo^{II/VI}$ materials catalyzed selectively the oxidation of the substrate to the

Table 4
Catalytic olefin oxidation using MS_n and MS heterogeneous catalysts and related homogeneous counterparts.

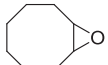
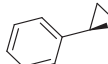
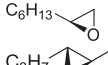
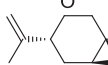
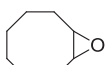
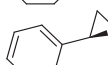
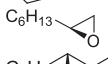
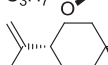
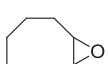
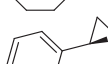
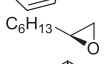
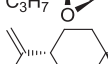
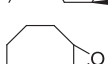
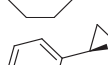
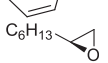
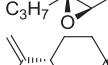
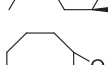
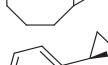
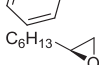
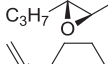
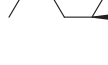
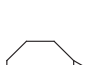
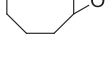
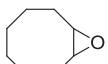
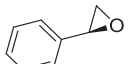
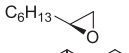
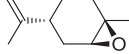
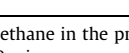
Entry	Catalyst	Epoxide ^a	TOF ($\times 10^3$) [$\text{mol mol}_{\text{Mo}}^{-1} \text{s}^{-1}$] ^b	Conv. (%) ^c	Sel. (%) ^d	ee (%) ^e
1	$Me_2bpy-Mo^{II}$		3	41	100	–
2			4	37	15	<5
3			77	67	100	<5
4			0.2	25	59	<5
5			15	56	91	<5 ^f
6	$Me_2bpy-Mo^{VI}$		2	53	100	–
7			0.3	16	45	<5
8			99	57	100	<5
9			1	28	71	<5
10			13	83	92	<5 ^f
11	$MS-bpy-Mo^{II}$		14	99	100	–
12			0.5	92	1	10
13			80	62	100	13
14			3	94	99	13
15			24	77	91	14 ^f
16	$MS-bpy-Mo^{VI}$		130	100	100	–
17			1	18	3	21
18			2	56	100	<5
19			6	94	97	11
20			11	27	74	15 ^f
21	$MS_n-bpy-Mo^{II}$		11/6/1 ^g	100/94/86 ^g	100/100/100 ^g	–
22			0.4	58	14	32
23			0.6	69	100	82
24			2	94	98	100
25			20/4/5 ^g	99/75/57 ^g	100/100/100 ^g	100/76/54 ^{f,g}
26			7	37 ^h	90	83 ^f
27			12	63 ⁱ	96	85 ^f
28	$MS_n-bpy-Mo^{VI}$		3	94	100	–

Table 4 (continued)

Entry	Catalyst	Epoxide ^a	TOF ($\times 10^3$) [$\text{mol mol}_{\text{Mo}}^{-1} \text{s}^{-1}$] ^b	Conv. (%) ^c	Sel. (%) ^d	ee (%) ^e
29			0.4	26	14	51
30			76	62	100	86
31			1	30	71	84
32			11	75	86	95 ^f
33			14	99 ^h	100	94 ^f
34			134	100 ⁱ	100	93 ^f

^a All reactions carried out in dichloromethane in the presence of 2 eq. of oxidant (tbhp) and 1 mol% of molybdenum catalyst at 328 K.

^b Turnover Frequency calculated after 10 min.

^c Calculated after 24 h.

^d Calculated as "Yield of epoxide"/"Conversion" \times 100%.

^e Determined by chiral GC.

^f Value refers do diastereomeric excess (de) of the trans form.

^g Values correspond to 1st, 2nd and 3rd catalytic runs.

^h Reaction carried out in ethanol at 353 K.

ⁱ Reaction carried out in toluene in 383 K.

corresponding epoxide, without formation of any by-products (Table 4, entries 21 and 28). The homogeneous counterpart complexes – $\text{Me}_2\text{bpy-Mo}^{\text{II}}$ and $\text{Me}_2\text{bpy-Mo}^{\text{VI}}$ – showed also conversion with complete selectivity in this transformation. For this set of catalysts, the results are similar to those reported previously by Kühn and Thiel for Mo^{VI} -related complexes and materials [47,61,62].

However, it is possible to observe that the yield obtained with the heterogeneous materials is much higher than for remaining catalysts – $\text{Me}_2\text{bpy-Mo}^{\text{II}}$ and $\text{Me}_2\text{bpy-Mo}^{\text{VI}}$ complexes. In the case of the heterogeneous catalysts $\text{MS}_h\text{-bpy-Mo}^{\text{II/VI}}$ and $\text{MS-bpy-Mo}^{\text{II/VI}}$ materials, cyclooctene epoxidation occurs generally in a complete fashion with the lowest conversion reaching 94% for $\text{MS}_h\text{-bpy-Mo}^{\text{VI}}$. Kinetic profiling of cyclooctene epoxidation shows that both $\text{MS}_h\text{-bpy-Mo}^{\text{II/VI}}$ materials present rapid and very high conversion profiles (Fig. 7). All other catalysts converted cyclooctene to the desired epoxide in yields with matching kinetics. In addition, it is not possible to rule out that Mo loading in MS_h materials (4.26% in $\text{MS}_h\text{-bpy-Mo}^{\text{II}}$ and 1.21% in $\text{MS}_h\text{-bpy-Mo}^{\text{VI}}$) has a direct influence in cyclooctene epoxide yield.

Epoxidation of 1-octene was also benchmarked given that it is harder to epoxidize as this is an unbranched terminal olefin being

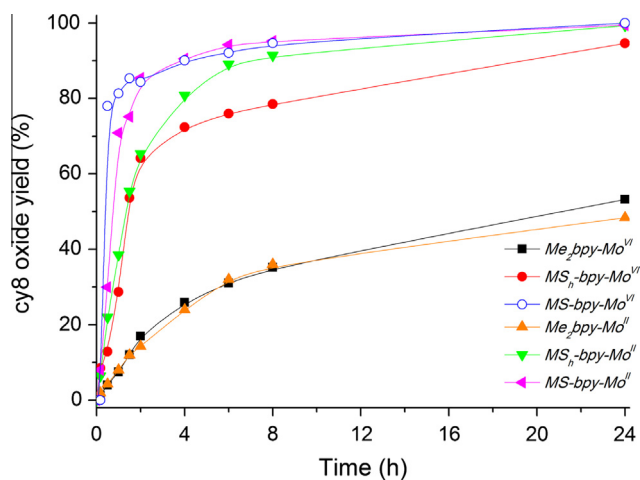


Fig. 7. Kinetics of cyclooctene epoxide yield in the presence of complexes $\text{Me}_2\text{bpy-Mo}^{\text{II}}$, $\text{Me}_2\text{bpy-Mo}^{\text{VI}}$, and materials $\text{MS}_h\text{-bpy-Mo}^{\text{II}}$, $\text{MS}_h\text{-bpy-Mo}^{\text{VI}}$, $\text{MS-bpy-Mo}^{\text{II}}$ and $\text{MS-bpy-Mo}^{\text{VI}}$.

therefore unactivated. Results confirm that all catalysts are also able to perform successfully such transformation, with conversions above 50%, showing complete selectivity to the required epoxide product. From results achieved, we found that, compared to the homogeneous complexes, the MS_h materials showed an extraordinary stereoselectivity. In fact, while the former did not show any ee of relevance, the latter made possible obtention of octane-1,2-epoxide as the sole product with quite a remarkable improvement in ee (an average of 84% for MS_h materials against less than 5% for complexes). On the other hand, the MS materials also show ee higher than the complexes, but not reaching the performance achieved by the MS_h counterparts (Table 4, entries 13, 18, 23, and 30).

Impelled by the promising results, we extended the test-set to more sensitive substrates – *trans*-hex-2-en-1-ol and *R*(+)-limonene – to evaluate both chemo- and stereoselectivity. According to Table 4, epoxidation of the former olefin led to the formation of hexan-1-ol-2,3-epoxide as major product in all catalytic systems tested. Once more, both MS_h heterogeneous catalysts exceeded the homogeneous counterparts for this substrate with $\text{MS}_h\text{-bpy-Mo}^{\text{II}}$ catalyst reaching almost reaction completeness with virtual absolute selectivity for the desired epoxide product (Table 4, entry 24). The same results were observed for the MS catalysts which show also very high substrate conversion yielding the epoxide as the major product. However, comparing the measured ee's, it can be observed that once more, the MS_h catalysts outperform the MS ones. In fact, the MS_h yield ee's of 100% and 84% for the Mo^{II} and Mo^{VI} derivatives, while the MS counterparts reach only 13% and 11%, by the same order.

The same trend was observed for *R*(+)-limonene. In this case, both MS_h heterogeneous catalysts display outstanding performance (Table 4, entries 25 and 32) where limonene epoxide was obtained not only in excellent yield but also with perfect stereoselectivity. The kinetic profiles are similar for all MS_h catalysts (Fig. 8). Although they do not show a rapid beginning, they convert the substrate to the desired product with good to excellent yield. However, and as already mentioned, the major advantage of the heterogeneous catalysts was shown by the resulting product stereoselectivity. Performance of the MS materials seems to follow the same trend in terms of substrate conversion and epoxide yield for limonene, as described above for MS_h counterparts. The exception seems to be once more stereoselectivity which is again very low when compared to the helical heterogeneous catalysts.

In an attempt to modulate conversion and selectivity for *R*-(+)-limonene epoxidation, the effects of solvent and temperature were tested as well using materials $MS_h\text{-bpy-Mo}^{II}$ and $MS_h\text{-bpy-Mo}^{VI}$ as catalysts. From the results in Fig. 9 (bottom), it is obvious that reactions in dichloromethane at 328 K lead to high substrate conversion in both cases. But in order to investigate whether the increase in the temperature with different solvents affected the results, we used ethanol and toluene. From the obtained results with different solvents, it is observed that material $MS_h\text{-bpy-Mo}^{II}$ is much more sensitive to different solvents than material $MS_h\text{-bpy-Mo}^{VI}$. According to Fig. 9 for the former, it is not ruled out that a different solvent with higher reaction temperature leads to better results in conversion and selectivity, like the $MS_h\text{-bpy-Mo}^{VI}$ counterpart or as observed for other catalysts described previously by our group [35,52,63].

When assessing catalytic performance of heterogeneous systems, it is important to evaluate catalyst stability in both terms of active center leaching and in recycling experiments. In this way, considering the first vector, active site leaching, we decided to run a catalytic cycle and remove the catalyst after 2 h reaction and keep following the reaction in the absence of the catalyst to evaluate possible leaching of Mo species to the slurry taking material $MS_h\text{-bpy-Mo}^{II}$ as catalyst. We found that after 2 h reaction, cyclooctene conversion is ca. 66%, but after removing the catalyst, the final conversion after 24 h reaches only 72% while that in the presence of the catalyst reaches 100% (Table 4, entry 21 and Fig. 7). It shows clearly that the reaction almost stops indicating that there is little or no leaching to the homogeneous phase. Such result makes possible to conclude that the catalysts are truly heterogeneous in nature.

The second vector was to evaluate catalyst performance in recycling experiments. Using once more material $MS_h\text{-bpy-Mo}^{II}$ as catalyst, we performed a test to understand how recyclable the catalyst is. Recycling was accomplished three times using cyclooctene or *R*-(+)-limonene as substrates (Table 4, entries 21 and 25). For both catalytic systems, loss of activity was found after each catalytic cycle by ca. 7% and 24% for each of the substrates, respectively. In more detail, cyclooctene conversion reached 100%, 94%, and 86%, whereas *R*-(+)-limonene conversion achieved 99%, 75%, and 57% over three consecutive cycles, although selectivity to the epoxide was not affected as shown in Fig. 9-top. Despite the epoxide selectivity was not affected, in the case of *R*-(+)-limonene, a deterioration of the *cis/trans* ratio over recycle (Table 4, entry 25) is observed. It should be mentioned that the catalyst was filtered, washed with dichloromethane, and dried prior to a new recycling experiment.

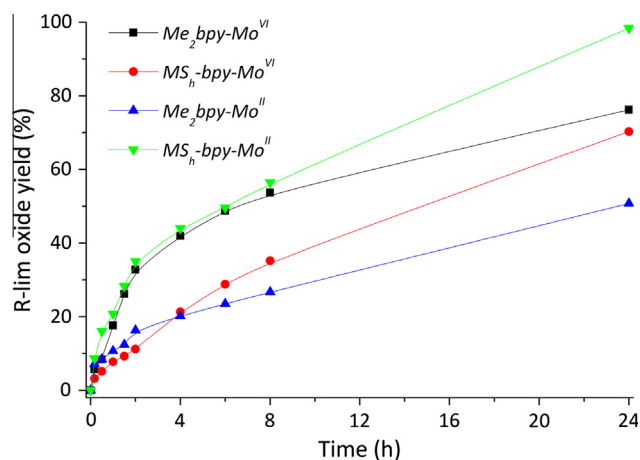


Fig. 8. Kinetics of *R*-(+)-limonene yield in the presence of complexes $Me_2bpy\text{-Mo}^{VI}$, $MS_n\text{-bpy-Mo}^{VI}$, and materials $MS_n\text{-bpy-Mo}^{II}$ and $MS_n\text{-bpy-Mo}^{VI}$.

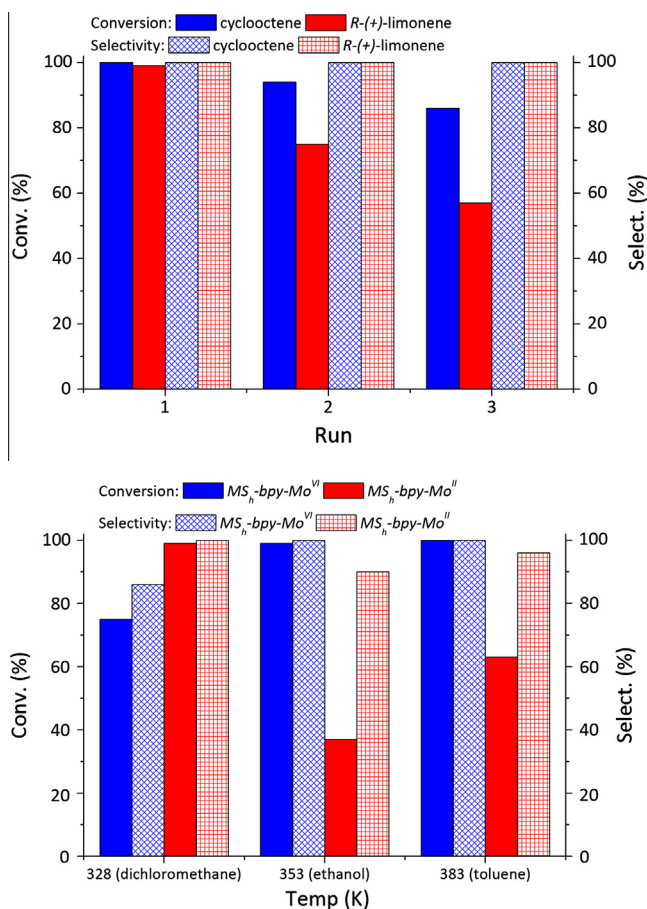


Fig. 9. Bottom – Conversion and selectivity for *R*-(+)-limonene in the presence of materials $MS_n\text{-bpy-Mo}^{II}$ and $MS_n\text{-bpy-Mo}^{VI}$ under variable temperature and solvent conditions after 24 h. Top – Conversion and selectivity for cyclooctene and *R*-(+)-limonene in the presence of material $MS_n\text{-bpy-Mo}^{II}$ as catalyst in recycling experiments after 24 h.

Concerning the initial catalytic activity calculated, turnover frequencies (TOF) after 10 min reaction time were found to fit in a wide range of values. This means that, apart from some exceptions, the reactions are initially slow, but after the 24 h, they achieve quite good results as discussed above. Despite this, for instance, for cyclooctene epoxidation, we report values that range between 2×10^{-3} and $3 \times 10^{-3} \text{ mol mol}^{-1} \text{ s}^{-1}$ for the complexes and between 1×10^{-3} and $130 \times 10^{-3} \text{ mol mol}^{-1} \text{ s}^{-1}$ for the materials. In the case of the $Me_2bpy\text{-Mo}^{II}$ complex, its TOF (2×10^{-3}) is lower than those found in the literature for related Mo^{II} complexes, which range between 68×10^{-3} and $91 \times 10^{-3} \text{ mol mol}^{-1} \text{ s}^{-1}$ with acetonitrile, nicotinic, and picolinic acids as ligands [52,64]. For the $Me_2bpy\text{-Mo}^{VI}$ complex, its value of $3 \times 10^{-3} \text{ mol mol}^{-1} \text{ s}^{-1}$ is found comparable to those reported by Kühn, using ionic liquids as solvent [47]. The heterogeneous catalysts show also TOF values that fit with values found in the literature [52,63,64], although there is one system in this discussion ($MS\text{-bpy-Mo}^{VI}$) that outperforms the literature systems. Such comparisons should be made with care, since our TOF values were measured after 10 min reaction time, whereas those found in the literature report TOF values after only 5 or 15 min reaction time.

In addition, the higher catalytic performance of the heterogeneous materials face to the homogeneous ones may be due to the higher surface acidity which may assist in substrate activation, a situation that cannot occur with the complexes. This effect has been described previously in the literature [35,65].

3.4. Origin of stereoselectivity

As evidenced by catalytic results for *trans*-hex-2-en-1-ol stereocontrol was achieved using the heterogeneous catalysts where the desired hexan-1-ol-2,3-epoxide product was obtained in an absolutely stereoselective way (Table 4, entry 24). The same is observed for 1-octene and *R*(+)-limonene epoxidation being a remarkable achievement using a simple catalytic system based on a symmetric-ligand molecular catalyst. Compared to the homogeneous counterparts, the *ee* obtained with the heterogeneous helical catalysts may arise from the rigid confined environment leading to substrate hindrance on approaching the catalytic active center in the confined space of the mesoporous helical host material. This arises from the described channel left-handedness in the original literature report and the fact that the grafted *bpy* ligand may lie at saddle shaped sites (cf. Fig. 3 in Ref. [32]) in the walls giving rise to a non-planar position of both *N*-donor atoms chelating Mo. This yields a confined environment imposed by the rigid inorganic matrix, which leads to enhanced stereocontrol over the catalytic reaction products.

Face to such positive results, we investigated whether the inorganic matrix has really chiral channels, adopting a literature procedure [51]. Based on that literature procedure to evaluate chirality of a given inorganic mesoporous material matrix, we have adsorbed enantiopure *D*-phenylalanine and *L*-phenylalanine into the porous system of MS_h materials [51]. According to the authors who reported the original synthesis of MS_h materials [32], the helical materials have left-handed channels. However, that conclusion was made based on TEM observations, and we think further evidence at the molecular level is required to make a proof of concept on chiral recognition.

Our results on the adsorption of enantiopure phenylalanine (*D* and *L*; with similar dimensions to the substrates used) show that MS_h materials selectively adsorb twice as much *D*-phenylalanine after 24 h, as evidenced in Fig. 10, showing a clear “preference” for *D*-phenylalanine over *L*-phenylalanine. This was found to be reproducible over 5 batches (each one run in triplicate) and strongly supports that the matrix is chiral. Compared to data from Ref. [51], arising from adsorption of *D*- and *L*-valine, our results show a greater discrimination between both enantiomers (phenylalanine in the present case). This is most probably due to the higher bulkiness of this molecule compared to valine. Nevertheless, it confirms the observed left-handedness chirality of the channels in the original synthesis of MS_h materials [32] and explains why reactions achieve the presented results. Attention should be drawn to the fact that in this work, we are probing channel chirality. As a

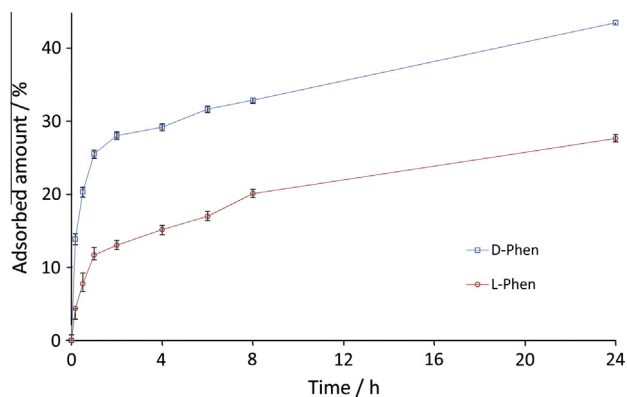


Fig. 10. Adsorption kinetic profiles of pure *L*-phenylalanine and *D*-phenylalanine on MS_h materials. The plot represents the average of 5 different batches each one tested in triplicate (error bars are also included).

matter of fact, in Ref. [32], authors mention channels as being chiral (confirmed in the present work), although the helical rods are not.

Statistical analysis on the results, evidenced by the small error bars, is also a good tool to demonstrate that the synthesis procedure of such materials is quite reproducible based on a simple entropy-driven mechanism [32]. Therefore, it strongly suggests that the inorganic matrix of MS_h materials is really chiral with focus on one predominant form. This study also confirms previous observations made by Han et al. in the original synthesis description where TEM data showed that MS_h materials are left-handed [32]. However, further investigation on the nature of the chirality of the inorganic matrix lie outside the scope of the present research and should be directed to the original reference [32].

Such confined space chiral concept imposed by the rigid inorganic backbone has been previously raised and discussed to explain similar *ee* enhancements [16–27], where reactants are allowed to approach in a single orientation. Data in Table 4 supports this assumption by the observation of higher stereoselectivity achieved for bulkier substrates. In this way, for MS_h catalysts, the trend is more or less, styrene < 1-octene < *trans*-hex-2-en-1-ol \approx *R*(+)-limonene. In addition, present data show that MS_h materials can really be used in processes where chiral recognition is valuable, such as catalysis or separation technology. This fact is corroborated by catalytic results arising from experiments using the *MS* set of materials which yielded low stereoselectivity results (see Table 4).

Surprisingly, there are some results of relevance achieved with *MS* materials. By the same token explained above for the MS_h counterparts, this may be due to the template extracting process. The HCl used to remove the template can etch the inner walls creating defects which may, to some extent, create local confined space which will hinder reactants approach. In this way, since the complexes are not chiral or asymmetric either, the most plausible reason for the reported results may be directly related to how the complexes graft onto the MS_h walls. In fact, if they graft in such a way that they can behave as pro-chiral catalysts which is imposed by the walls of the chiral channels then it would result in a high degree of steric hindrance which render several restrictions on how the organic reactants approach the metal active center. To further support this thesis, results from the recycling experiments show that stereoselectivity decreases concomitantly. This may be related to the well-known issue that mesoporous materials suffer wall degradation by an etching process when exposed to aggressive conditions [66]. In this way, the channels will start to lose their chirality and the steric restrictions once existed may no longer exist, thus leading to the stereoselectivity loss.

4. Conclusion

In conclusion, we describe the first use of chiral helical mesoporous materials as heterogeneous catalysts for asymmetric olefin epoxidation based on molybdenum active sites. Although previous use of such MS_h materials was reported in catalytic applications, no mention to stereocontrol has been made [67,68]. As a major achievement, these catalysts offer an outstanding stereocontrol of the reaction products arising from confined space imposed by the rigid inorganic chiral backbone. In addition, these catalysts were found to be very effective under several circumstances. For instance, they can oxidize unactivated unbranched terminal olefins (1-octene) with good performance. Although leaching does not occur to a great extent, recyclability seems to be a drawback, although after three cycles, they are still more efficient than the homogeneous counterparts. The excellent stereocontrol of the epoxidation reaction seems to be intrinsically related with

confinement effects imposed by the chiral inorganic backbone which modulates the way reactants approach active sites. This arises from experimental data confirming the chirality of the inorganic matrix which selectively adsorbs a given enantiomer over another. Despite this, recycling experiments also evidence a deterioration of stereoselectivity which may be related to the degradation of the chiral channel system of the host materials, which is known to occur under aggressive conditions.

This is certainly an important contribution for such concept and may render such materials further applications where chiral recognition is important.

Acknowledgments

Authors thank FCT, POCI and FEDER (Projects PTDC/QUI/71576/767 2006, PEst-OE/QUI/UI0612/2013, RECI/QEQ-QIN/0189/2012 and PEst-OE/QUI/UI0100/2013), M.S.S. thanks FCT for a research Grant (SFRH/BD/48640/2008).

We would like to thank the Editor of Journal of Catalysis, Prof. S.T. Oyama and all the referees, for many pertinent and timely suggestions that contributed for a better discussion of data.

Appendix A. Supplementary material

Supplementary data associated with this article can be found, in the online version, at <http://dx.doi.org/10.1016/j.jcat.2013.08.032>.

References

- [1] A. Taguchi, F. Schüth, *Micropor. Mesopor. Mater.* 77 (2005) 1.
- [2] M.H. Valkenberg, W.F. Hölderich, *Catal. Rev. – Sci. Eng.* 44 (2002) 321.
- [3] F. Hoffmann, M. Cornelius, J. Morell, M. Fröba, *Angew. Chem. Int. Ed. Engl.* 45 (2006) 3216.
- [4] T. Katsuki, K.B. Sharpless, *J. Am. Chem. Soc.* 102 (1980) 5974.
- [5] Y. Gao, R.M. Hanson, J.M. Klunder, S.Y. Ko, H. Masamune, K.B. Sharpless, *J. Am. Chem. Soc.* 109 (1987) 5765.
- [6] R. Irie, K. Noda, Y. Ito, N. Matsumoto, T. Katsuki, *Tetrahedron Lett.* 31 (1990) 7345.
- [7] W. Zhang, J.L. Loebach, S.R. Wilson, E.N. Jacobsen, *J. Am. Chem. Soc.* 112 (1990) 2801.
- [8] Q.-H. Xia, H.-Q. Ge, C.-P. Ye, Z.-M. Liu, K.-X. Su, *Chem. Rev.* 105 (2005) 1603.
- [9] M. Shibasaki, H. Sasai, T. Arai, *Angew. Chem. Int. Ed. Engl.* 36 (1997) 1236.
- [10] M.J. Porter, J. Skidmore, *Chem. Commun.* (2000) 1215.
- [11] D. Díez, M.G. Núñez, A.B. Antón, P. García, R.F. Moro, N.M. Garrido, I.S. Marcos, P. Basabe, J.G. Urones, *Curr. Org. Synth.* 5 (2008) 186.
- [12] Y. Shi, *Acc. Chem. Res.* 37 (2004) 488.
- [13] M. Hickey, D. Goettel, Z. Crane, Y. Shi, *Proc. Natl. Acad. Sci. USA* 101 (2004) 5794.
- [14] S. Juliá, J. Masana, J.C. Vega, *Angew. Chem. Int. Ed. Engl.* 19 (1980) 929.
- [15] S. Juliá, J. Guixer, J. Masana, J. Rocas, S. Colonna, R. Annuziata, H. Molinari, *J. Chem. Soc. Perkin Trans. 1* (1982) 1317.
- [16] J. Wang, L. Zhao, H. Shi, J. He, *Angew. Chem. Int. Ed. Engl.* 50 (2011) 9171.
- [17] M.D. Jones, R. Raja, J.M. Thomas, B.F.G. Johnson, D.W. Lewis, J. Rouzaud, K.D.M. Harris, *Angew. Chem. Int. Ed. Engl.* 42 (2003) 4326.
- [18] R. Raja, J.M. Thomas, M.D. Jones, B.F.G. Johnson, D.E.W. Vaughan, *J. Am. Chem. Soc.* 125 (2003) 14982.
- [19] M.R. Castillo, L. Fousse, J.M. Fraile, J.I. García, J.A. Mayoral, *Chem. Eur. J.* 13 (2007) 287.
- [20] J.M. Fraile, J.I. García, C.I. Herreras, J.A. Mayoral, M.A. Harmer, *J. Catal.* 221 (2004) 532.
- [21] J.M. Fraile, J.I. García, C.I. Herreras, J.A. Mayoral, O. Reiser, A. Socullamos, H. Werner, *Chem. Eur. J.* 10 (2004) 2997.
- [22] R.A. García, V. Morales, T. Garcés, *J. Mater. Chem.* 22 (2012) 2607.
- [23] R.A. García, R. van Grieken, J. Iglesias, V. Morales, N. Villajos, *J. Catal.* 274 (2010) 221.
- [24] T. Yamamoto, M. Sugimoto, *Angew. Chem. Int. Ed. Engl.* 48 (2009) 539.
- [25] T. Yamamoto, T. Yamada, Y. Nagata, M. Sugimoto, *J. Am. Chem. Soc.* 132 (2010) 7899.
- [26] T. Yamamoto, Y. Akai, Y. Nagata, M. Sugimoto, *Angew. Chem. Int. Ed. Engl.* 50 (2011) 8844.
- [27] Y. Nagata, S. Ohashi, M. Sugimoto, *J. Polym. Sci. Part A: Polym. Chem.* 50 (2012) 1564.
- [28] T. Gier, X. Bu, P. Feng, G.D. Stucky, *Nature* 395 (1998) 154.
- [29] D. Bradshaw, T.J. Prior, E.J. Cussen, J.B. Claridge, M.J. Rosseinsky, *J. Am. Chem. Soc.* 126 (2004) 6106.
- [30] A.E. Rowan, R.J.M. Nolte, *Angew. Chem. Int. Ed. Engl.* 37 (1998) 63.
- [31] S. Che, Z. Liu, T. Ohsuna, K. Sakamoto, O. Terasaki, T. Tatsumi, *Nature* 429 (2004) 281.
- [32] Y. Han, L. Zhao, J.Y. Ying, *Adv. Mater.* 19 (2007) 2454.
- [33] D. Trong-On, D. Desplandier-Giscard, C. Danumah, S. Kaliaguine, *Appl. Catal. A* 222 (2001) 299.
- [34] A.M. Balu, J.M. Hidalgo, J.M. Campelo, D. Luna, R. Luque, J.M. Marinas, A.A. Romero, *J. Mol. Catal. A: Chem.* 293 (2008) 17.
- [35] N.U. Silva, C.I. Fernandes, T.G. Nunes, M.S. Saraiva, C.D. Nunes, P.D. Vaz, *Appl. Catal. A* 408 (2011) 105.
- [36] N. Grover, F.E. Kühn, *Curr. Org. Chem.* 16 (2012) 16.
- [37] M.R. Maurya, *Curr. Org. Chem.* 16 (2012) 73.
- [38] P.D. Vaz, C.D. Nunes, *Curr. Org. Chem.* 16 (2012) 89.
- [39] C.D. Nunes, P.D. Vaz, in: A.C. Poehler (Ed.), *Homogeneous Catalysts: Types, Reactions and Applications*, Nova Science Publishers Inc., New York, 2011, p. 43.
- [40] A.J. Burke, *Coord. Chem. Rev.* 252 (2008) 170.
- [41] F.E. Kühn, A.M. Santos, M. Abrantes, *Chem. Rev.* 106 (2006) 2455.
- [42] A.U. Barlan, A. Basak, H. Yamamoto, *Angew. Chem. Int. Ed. Engl.* 45 (2006) 5849.
- [43] A.U. Barlan, W. Zhang, H. Yamamoto, *Tetrahedron* 63 (2007) 6075.
- [44] N.U. Silva, T.G. Nunes, M.S. Saraiva, M.S. Shalamzari, P.D. Vaz, O.C. Monteiro, C.D. Nunes, *Appl. Catal. B* 113–114 (2012) 180.
- [45] P.K. Baker, *Chem. Soc. Rev.* 27 (1998) 125.
- [46] W.M. Carmichael, D.A. Edwards, G.W.A. Fowles, P.R. Marshall, *Inorg. Chem. Acta* 1 (1967) 93.
- [47] D. Betz, W.A. Herrmann, F.E. Kühn, *J. Organomet. Chem.* 694 (2009) 3320.
- [48] N. Garelli, P. Vierling, *J. Org. Chem.* 57 (1992) 3046.
- [49] M. Kruk, M. Jaroniec, A. Sayari, *Langmuir* 13 (1997) 6267.
- [50] M. Kruk, V. Antochshuk, M. Jaroniec, A. Sayari, *J. Phys. Chem. B* 103 (1999) 10670.
- [51] Z. Guo, Y. Du, Y. Chen, S.-C. Ng, Y. Yang, *J. Phys. Chem. C* 114 (2010) 14353.
- [52] A.C. Ventura, C.I. Fernandes, M.S. Saraiva, T.G. Nunes, P.D. Vaz, C.D. Nunes, *Curr. Inorg. Chem.* 1 (2011) 156.
- [53] B. Marler, U. Oberhagemann, S. Voltmann, H. Gies, *Micropor. Mater.* 6 (1996) 375.
- [54] W. Hammond, E. Prouzet, S.D. Mahanti, T.J. Pinnavaia, *Micropor. Mesopor. Mater.* 27 (1999) 19.
- [55] S.J. Gregg, K.S.W. Sing, *Adsorption, Surface Area and Porosity*, second ed., Academic Press, London, 1982.
- [56] M.D. Alba, A. Becerro, J. Klinowski, *J. Chem. Soc., Faraday Trans.* 92 (1996) 849.
- [57] A.A. Romero, M.D. Alba, W. Zhou, J. Klinowski, *J. Phys. Chem. B* 101 (1997) 5294–5300.
- [58] M. Kruk, M. Jaroniec, *Langmuir* 15 (1999) 5410.
- [59] P.D. Vaz, C.D. Nunes, M. Vasconcelos-Dias, M.M. Nolasco, P.J.A. Ribeiro-Claro, M.J. Calhorda, *Chem. Eur. J.* 13 (2007) 7874.
- [60] W. Bett, S. Cradoc, *Monatsh. Chem.* 111 (1980) 193.
- [61] J. Tang, L. Wang, G. Liu, Y. Liu, Y. Hou, W. Zhang, M. Jia, W.R. Thiel, *J. Mol. Catal. A* 313 (2009) 31.
- [62] C.D. Nunes, A.A. Valente, M. Pillinger, A.C. Fernandes, C.C. Romão, J. Rocha, I.S. Gonçalves, *J. Mater. Chem.* 12 (2002) 1735.
- [63] M. Vasconcelos-Dias, C.D. Nunes, P.D. Vaz, P. Ferreira, P. Brandão, V. Félix, M.J. Calhorda, *J. Catal.* 256 (2008) 301.
- [64] M. Vasconcelos-Dias, S.R.M.M. de Aguiar, C.D. Nunes, P.D. Vaz, T.G. Nunes, M.J. Calhorda, *Curr. Inorg. Chem.* 1 (2011) 146.
- [65] C.D. Nunes, A.A. Valente, M. Pillinger, J. Rocha, I.S. Gonçalves, *Chem. Eur. J.* 9 (2003) 4380.
- [66] A. Galarneau, M. Nader, F. Guenneau, F. Di Renzo, A. Gedeon, *J. Phys. Chem. C* 111 (2007) 8268.
- [67] A.I. Carrillo, E. Serrano, J.C. Serrano-Ruiz, R. Luque, J. Garcia-Martinez, *Appl. Catal. A: Gen.* 435–436 (2012) 1.
- [68] A.I. Carrillo, E. Serrano, R. Luque, J. Garcia-Martinez, *Chem. Commun.* 46 (2010) 5163.